Optical Pumping in Rubidium

Ishaan Aggarwal
Simon Fraser University

Abstract

This research investigates optical pumping, a process involving light-induced electron transitions in atoms, with a specific focus on rubidium isotopes Rb87 and Rb85. The study explores hyperfine splitting and the Zeeman effect under weak magnetic fields. A notable aspect of the experiment is the analysis of transient effects elicited through a square RF signal. Key findings include the determination of Gyromagnetic ratios: $2.07 \times 10^{-5} \pm 0.03 \times 10^{-5}$ for Rb87, and $3.0 \times 10^{-5} \pm 0.2 \times 10^{-5}$ for Rb85. These results closely match theoretical predictions, enhancing the understanding of atomic behavior in magnetic fields.

1 Introduction

Optical pumping, a technique that was first introduced by Alfred Kastler in the early 1950s, is a process that uses light to transition electrons from a lower energy state to a higher one within an atom. This interaction between light and matter leads to a non-equilibrium state within the atomic levels, known as a population inversion[5], when the majority of the system's constituents are in these excited states. Optical pumping is also used to cyclically pump electrons bound within an atom or molecule to a well-defined quantum state. For the simplest case of coherent two-level optical pumping of an atomic species containing a single outer-shell electron, this means that the electron is coherently pumped to a single hyperfine sublevel[4]. The frequency and polarization of the pump laser determine the sublevel in which the atom is oriented. In practice, completely coherent optical pumping may not occur due to power-broadening of the linewidth of a transition and undesirable effects such as hyperfine structure trapping and radiation trapping. Therefore the orientation of the atom depends more generally on the frequency, intensity, polarization, and spectral bandwidth of the laser as well as the linewidth and transition probability of the absorbing transition[6].

This technique has been instrumental in manipulating the quantum states of atoms and has found its place in the advancement of various technologies and research fields. Its applications are diverse, including the operation of lasers, atomic clocks, and Magnetic Resonance Imaging (MRI), and mostly prevalent in lasers. In the field of lasers, optical pumping is used to achieve a population inversion in the medium, which amplifies the emission of light for a specific range of optical frequencies. In atomic clocks, optical pumping prepares atoms in a specific quantum state before they undergo the hyperfine transition.

The goal of this report is to establish the Landé g factors and the Gyromagnetic ratios of the rubidium isotopes, Rb^{87} and Rb^{85}. These isotopes are subject to optical pumping, which is utilized to observe the hyperfine structure and Zeeman effects within the isotopes. A study conducted by the Department of Physics at the University of Cornell [6] reported the Landé g factors as 0.501 for Rb^{87} and 0.335 for Rb^{85}.

2 Theory

Alkali atoms, similar to the hydrogen atom, have a single electron in their outer shell, which dominates their chemical properties. Their electronic configuration, akin to hydrogen, simplifies the study of atomic structure and electron behavior 1[1]. The valence electron in these atoms experiences both the orbital angular momentum (L) and the spin angular momentum (S). These momenta, coupled through spin-orbit interaction, result in total angular momentum (J). This understanding is crucial for grasping how alkali atoms interact with external fields, including light. The interaction of alkali atoms with external fields, particularly light, is crucial due to their unique atomic structure. The single electron in the outer shell of alkali atoms determines their interaction with light. When light of a specific frequency interacts with these atoms, it can cause the outer electron to jump to a higher energy level, a process central to optical pumping. Additionally, the interaction with magnetic fields, as in the Zeeman effect[3], can lead to the splitting of energy levels, which is observable and crucial for understanding atomic behavior in various fields, including spectroscopy and quantum mechanics

In the context of alkali atoms, the Zeeman effect arises when a weak external magnetic field interacts with the energy levels of these atoms, leading to their further splitting. A "weak" magnetic field is defined as one where the resulting splitting of the energy levels is very small compared to the Hyperfine Splitting (HFS). This effect is fundamental in experiments involving alkali atoms as it helps in understanding the atomic structure and behavior under the influence of external magnetic fields.

The Zeeman effect can be visualized by a vector dia-

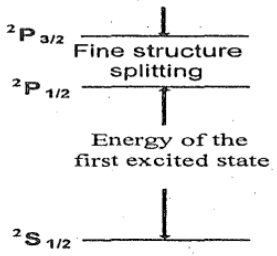

Figure 1: Energy level diagram of an alkali atom showing the fine structure splitting between the 2P1/2 and 2P3/2 states. Note: The diagram is not to scale; the fine structure splitting is significantly smaller than the energy difference between the ground state and the first excited state.

gram where the magnetic field $\mathbf{B}$ interacts with the total angular momentum $\mathbf{F}$ of the atom. As depicted in Figure[2] 2, the Zeeman effect in alkali atoms results from the interaction of a weak external magnetic field with the atomic energy levels, leading to their further splitting. This effect is crucial for understanding the atomic structure and behavior under magnetic fields. The component of $\mathbf{F}$ in the direction of the magnetic field, denoted as $\mathbf{M}$, precesses about the field at the Larmor frequency. This interaction is described by a Hamiltonian that accounts for the electronic and nuclear magnetic moments with the external field.

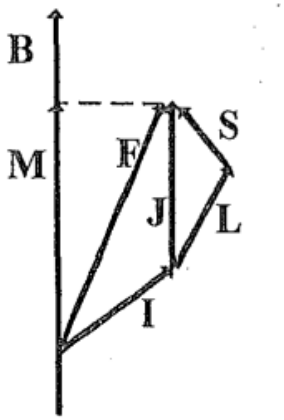

Figure 2: Vector diagram illustrating the Zeeman effect in an alkali atom. The magnetic field $\mathbf{B}$ interacts with the total angular momentum $\mathbf{F}$ of the atom, with the component $\mathbf{M}$ precessing about $\mathbf{B}$ at the Larmor frequency.

In alkali atoms, photon absorption is a critical process where light induces electronic transitions. These atoms absorb light of specific frequencies that match the energy differences between allowed transitions. The selection rules for these transitions typically follow the criteria: $\Delta L = 0, \pm 1$ and $\Delta J = 0, \pm 1$, but not $L = 0$ to $L = 0$. This means transitions can occur from the ground state to both of the excited states in alkali atoms.

Electric dipole transitions, the most common type in photon absorption, are governed by these selection rules and involve the conservation of angular momentum. When an alkali atom absorbs a photon, its electron transitions to a higher energy state, absorbing energy equivalent to the photon's energy. This absorption process is central to optical pumping, where the excitation of electrons is a preliminary step.

After absorption, atoms in the excited state eventually decay back to the ground state, emitting photons in the process. This cycle of absorption and emission is fundamental to understanding the interaction of light with atomic systems, and it plays a significant role in phenomena like fluorescence and the generation of coherent light in lasers.

As illustrated in Figure[8] 3, the absorption of light by alkali atoms involves specific transitions where electrons are excited to higher energy states. This process is crucial for initiating the optical pumping mechanism in these atoms.

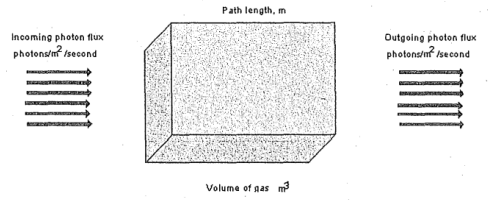

Figure 3: Light absorption by a volume of gas, demonstrating the process of photon absorption in alkali atoms, where incident light resonant with atomic transitions is absorbed, leading to the excitation of atoms.

Optical pumping in rubidium atoms is a delicate process influenced by both the specific characteristics of rubidium and the experimental setup. A direct current (DC) magnetic field is applied along the optical axis of the absorption cell, and transitions within the rubidium sample are induced by a transverse radio-frequency (RF) magnetic field. This setup results in the alignment of the magnetic quantum number $\mathbf{M}$ of rubidium's total angular momentum $\mathbf{F}$ along the DC magnetic field. This vector, $\mathbf{M}$, precesses around the applied magnetic field at the Larmor frequency, a phenomenon fundamental to the optical pumping process.

In optical pumping, the transitions between electronic energy levels are driven by optical radiation, and transitions between Zeeman levels are induced by the RF magnetic field. For instance, in rubidium-87 (Rb87) which has a nuclear spin of 3/2, these transitions are crucial for achieving the desired state of polarization or alignment in the atomic ensemble.

The role of buffer gases in this process cannot be overstated. Buffer gases are used to prevent the rubidium atoms from interacting with the container walls or with each other, which can lead to depolarization and loss of the pumped state. By stabilizing the atomic environment, buffer gases help maintain the effectiveness of optical

pumping. As shown in Figure[7] 4

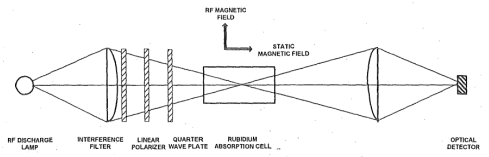

Figure 4: Magnetic fields and angular momenta in the optical pumping of rubidium, illustrating the alignment of angular momenta and the magnetic field interactions.

After establishing the foundational concepts of atomic structure, the Zeeman effect, and the principles of optical pumping, we now turn our attention to the more quantifiable aspects of these phenomena, specifically focusing on the Larmor frequency and the Gyromagnetic ratio. These concepts are not only pivotal in understanding the atomic behavior under magnetic fields but also in calculating specific measurable outcomes in our experiment.

The Larmor frequency, represented as ω_0, is crucial in describing the precession of atomic magnetic moments in an external magnetic field. It is expressed by:

$$\omega_0 = \gamma B_{\text{RF}}, \tag{1}$$

where B_{RF} is the magnetic field strength from the radio-frequency source, and γ signifies the Gyromagnetic ratio, a key factor linking atomic magnetic moments to angular momentum.

This Gyromagnetic ratio is intricately related to the Landé g-factor, g_F, a dimensionless quantity indicating the magnetic moment in quantum terms. The Gyromagnetic ratio equation is given by:

$$\gamma = \frac{g_F \mu_0}{h}, \tag{2}$$

where μ_0 is the Bohr magneton, and h is Planck's constant. Understanding the variations in the g-factor between different isotopes, such as Rb85 and Rb87, is a focal point of our study.

The period of transient effects observed during changes in the RF field, denoted as T, inversely correlates with the Larmor frequency, underscoring the atomic system's sensitivity to magnetic field strength. The period is calculated by:

$$T = \frac{1}{\gamma B_{\text{RF}}}, \tag{3}$$

This relationship is crucial for analyzing the transient phenomena in our experiment.

Our primary objective is the calculation of the g-factor for Rb85 and Rb87 isotopes. The measurement of the time period ratios of transient effects between these isotopes will enable us to ascertain their respective g-factors. We anticipate that the theoretical ratio should be approximately $\frac{3}{2}$, mirroring the known differences in the g-factors of these isotopes. This calculation is essential for a deeper understanding of atomic properties under magnetic fields and has significant implications in quantum mechanics and spectroscopy.

Transient phenomena in optical pumping are particularly noteworthy when there are rapid changes in the radio-frequency (RF) field. These transient effects provide crucial insights into the dynamic behavior of atoms under varying conditions and are key to understanding the responsiveness of the atomic system to external stimuli. When the RF field applied to an atom changes rapidly, the atomic states do not immediately adjust to the new conditions. Instead, there is a delay as the atoms transition between energy levels, leading to transient phenomena. These effects are observed as temporary imbalances in population distribution among the atomic energy levels and fluctuations in the emitted or absorbed light.

3 Experimental Methods

The experimental setup for optical pumping, illustrated in Figure 4, begins with an RF discharge lamp. This lamp, containing xenon gas and rubidium metal, is critical for generating the energy necessary to excite rubidium atoms. Positioned in front of the lamp is an interference filter that selectively allows wavelengths of 780 nm and 795 nm to pass, crucial for the experiment.

Central to the setup is the rubidium cell, encased by various solenoid coils. A vertical solenoid applies an RF magnetic field, while two horizontal solenoids manage a direct current field. The sweep field coil, with its specific design and wire turns, plays a vital role in generating an effective magnetic field.

Optical detection is achieved through a convex lens that converges light onto a detector connected to an optical pumping unit. This unit amplifies the signals for oscilloscope visualization.

An essential part of the experiment is measuring the absorption cross-section of rubidium. This is conducted by adjusting the temperature of the rubidium cell and recording the detector's voltage response. The data obtained is crucial for comparing the experimental cross-section values with theoretical predictions.

The table 1 displays the atomic density of rubidium at various temperatures, integral to determining the cross-section. This temperature-dependent behavior of rubidium atoms provides insights into their absorption characteristics.

Prior to RF resonance measurements, it's crucial to counteract external magnetic fields, like Earth's magnetic field. A gaussmeter is employed for this purpose, and the apparatus is aligned accordingly. The horizontal sweep field is finely tuned around zero to isolate specific rubidium isotopes' responses.

Calibration of the magnetic field is meticulously carried out, using measurements and adjustments tailored to each rubidium isotope. This calibration is based on theoretical equations 1 from the theory section.

Temperature (K)	Density (atoms/cubic meter)
290	3.3×10^{15}
300	1.1×10^{16}
310	2.9×10^{16}
320	7.5×10^{16}
330	1.8×10^{17}
340	4.3×10^{17}
350	8.3×10^{17}
360	1.5×10^{18}
370	3.7×10^{18}
380	6.3×10^{18}
390	1.2×10^{19}
400	2.4×10^{19}

Table 1: Atomic density of solid or liquid rubidium as a function of temperature.

The quadratic Zeeman effect, another experimental focus, is observed by adjusting the RF signal and magnetic field settings. The oscilloscope readings during these adjustments provide valuable data.

Lastly, transient effects are explored by modulating the RF signal. Observing the system's response to these changes, especially the oscillations in the signal, sheds light on the atomic dynamics under rapid changes in conditions.

4 Results and Discussion

In our study, the calibration of the sweep and main coils was meticulously conducted. The sweep coil calibration, as depicted in Figure 5, involved measuring the current and magnetic field with varying RF signals. This process revealed a linear relationship between the magnetic field from the sweep coil and the direct current, yielding a slope of 0.714 ± 0.003 and an intercept of -0.010 ± 0.001.

Similarly, the calibration of the main coils was carried out using varying currents, with the findings illustrated in Figure 6. This calibration demonstrated a slope of 8.1 ± 0.1 and an intercept of -0.010 ± 0.001 for the magnetic field versus direct current relationship, indicating the precision and consistency of our experimental setup.

As depicted in Figure 7, the voltage data and its corresponding fitted model, based on equation 1, are presented. This voltage data represents the light absorption measurements taken during the process of heating the rubidium sample. The heating process involved increasing the temperature in increments of 10K until a maximum of 300K was reached. The final optimized values obtained were $I_o = 0.7609 \pm 0.0004$ and $\sigma_{ol} = 0.04448 \pm 0.00003$. Given that the rubidium cell has a length, l, of 2.5cm, the cross-section, σ_o, was calculated to be $1.779 \times 10^{-16} \pm 0.001 \times 10^{-16} m^2$. Upon comparison with the theoretical cross-section, it was found that the experimental value is an order of magnitude smaller.

The experiment accurately pinpointed zero field resonance at a sweep field current of 0.144 A. Through careful application of coil parameters, as detailed in Section 3, the residual magnetic field was determined to be 0.087 gauss. This precision underpins the experiment's ability to measure subtle magnetic effects on atomic behavior. For both Rb87 and Rb85 isotopes, the sweep field currents at an RF frequency of 150 kHz resulted in magnetic fields of 0.209 ± 0.04 gauss for Rb87 and 0.314 ± 0.05 gauss for Rb85. The derived g-factors, 0.51 ± 0.01 for Rb87 and 0.34 ± 0.06 for Rb85, exhibited concordance with theoretical values, reflecting the precision of the experimental setup.

Additional g-factor measurements, depicted in Figure 8, revealed the transition frequencies of rubidium atoms as a function of the sweep coil currents. The slopes obtained, 0.438 ± 0.002 for Rb87 and 0.291 ± 0.001 for

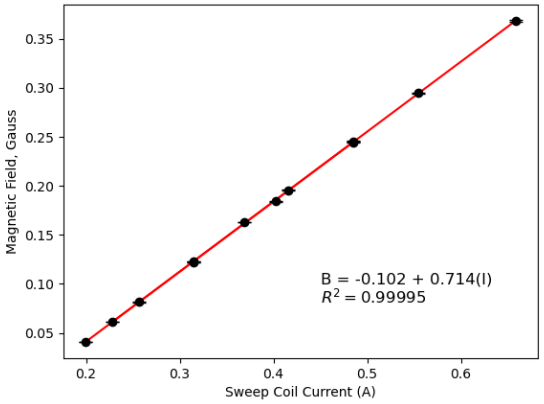

Figure 5: Graph showcasing the magnetic field variation in relation to sweep coil current. The experimental data, marked by black dots with error bars, demonstrate the magnetic field's dependence on the current. The linear fit, in red, results in a slope of 0.714 ± 0.003 and an intercept of -0.010 ± 0.001.

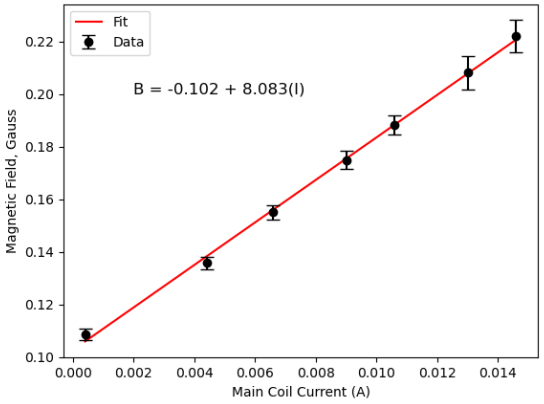

Figure 6: Plot of magnetic field against main current for main coils, illustrated with black dots and error bars. The red linear fit indicates a slope of 8.1 ± 0.1 and an intercept of -0.010 ± 0.001.

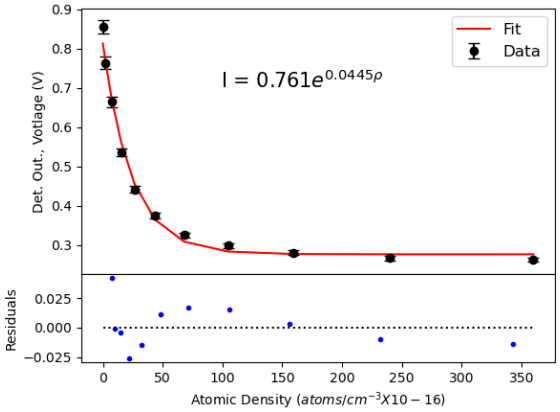

Figure 7: Graph showing detector voltage correlated with the density of rubidium atoms. Black dots represent experimental data with error bars, while the theoretical model is depicted by a continuous red line.

Rb85, and their ratio of 1.51 ± 0.01, aligned remarkably with the theoretical g-factor ratio of 1.5. This agreement reinforces the reliability of the experimental methods and the consistency of the results with established quantum mechanical principles.

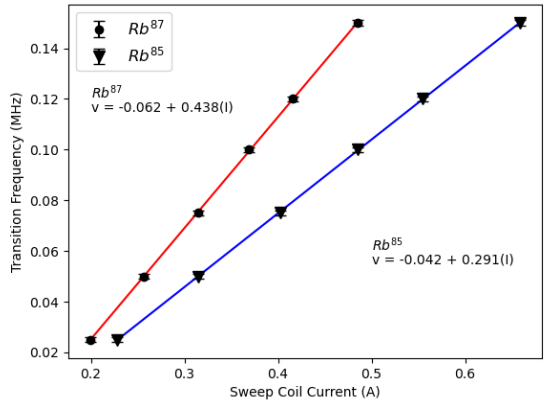

Figure 8: Graph depicting the transition frequencies of Rb^{87} and Rb^{85} isotopes against the sweep coil current. In the graph, Rb^{87} is represented by black circles and Rb^{85} by inverted triangles. Linear fits are shown, with Rb^{87}'s in red and Rb^{85}'s in blue, highlighting their magnetic response differences. The derived slopes are 0.438 ± 0.002 for Rb^{87} and 0.291 ± 0.001 for Rb^{85}, with corresponding intercepts of -0.062 ± 0.002 for Rb^{87} and -0.042 ± 0.001 for Rb^{85}.

In the experiment, a magnetic field of 2.174 gauss was effectively applied to the rubidium cell using the main coil. We observed the Quadratic Zeeman effects for Rb^{87} and Rb^{85} isotopes at specific RF frequencies of 4.9 MHz and 3.3 MHz, respectively. Figure 9 captures the dynamic light absorption profiles of these isotopes as the magnetic field from the sweep coil was varied. The illustration clearly shows Rb^{87} in red and Rb^{85} in blue, with each color representing the light absorption of the corresponding isotope. The graph effectively highlights multiple transitions at different energy levels for both isotopes, underscoring the complexities inherent in their energy states when subjected to varying magnetic fields.

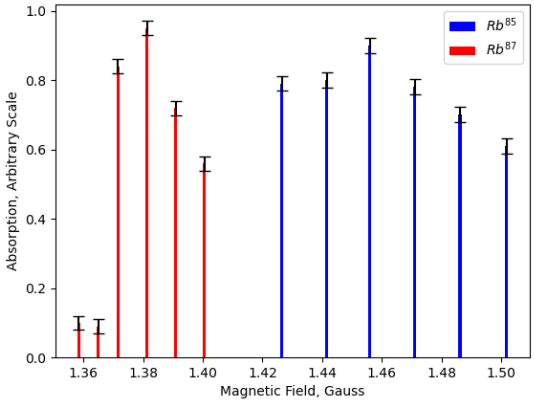

Figure 9: Depiction of light absorption in response to varying magnetic fields, with Rb^{87} represented in red and Rb^{85} in blue.

Transient effects in rubidium atoms were noted upon applying a square RF signal. This phenomenon is depicted in Figure 10, showcasing the variation in the time period for electronic transitions from higher to lower states as influenced by the increasing RF magnetic field. Crucially, this data facilitated the calculation of the Gyromagnetic ratios for the isotopes. For Rb^{87}, the ratio was found to be $2.07 \times 10^{-5} \pm 0.03 \times 10^{-5}$, and for Rb^{85}, it was $3.0 \times 10^{-5} \pm 0.2 \times 10^{-5}$. Notably, the ratio of these values, 1.45 ± 0.09, closely aligns with the theoretical ratio expected between Rb^{87} and Rb^{85} isotopes.

5 Conclusion

The calibration of the sweep and main coils was a crucial aspect of our experiment. The sweep coil calibration exhibited a slope of 0.714 ± 0.003 and an intercept of -0.010 ± 0.001, while the main coil calibration showed a slope of 8.1 ± 0.1 and the same intercept. The precise identification of zero field resonance at a sweep field current of 0.144 A, with a residual field of 0.087 gauss, was significant. Furthermore, the g-factor calculations for Rb^{87} and Rb^{85} isotopes, yielding 0.51 ± 0.01 and 0.34 ± 0.06 respectively, corroborated well with theoretical expectations. The observation of the Quadratic Zeeman effects at RF signals of 4.9 MHz for Rb^{87} and 3.3 MHz for Rb^{85}, alongside the transient effects leading to Gyromagnetic ratios of $2.07 \times 10^{-5} \pm 0.03 \times 10^{-5}$ for Rb^{87} and $3.0 \times 10^{-5} \pm 0.2 \times 10^{-5}$ for Rb^{85}, further demonstrated the experiment's effectiveness. The ratio of 1.45 ± 0.09 for these Gyromagnetic ratios closely matched

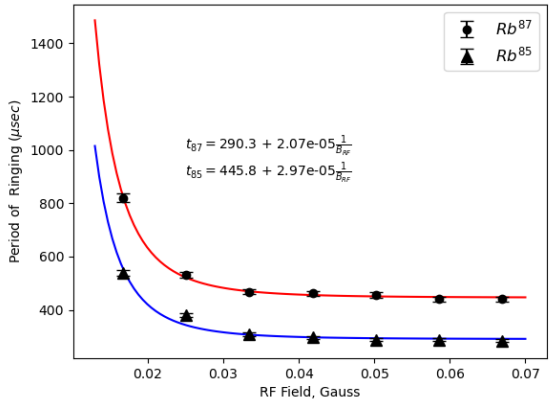

Figure 10: Graph showing the period of ringing in microseconds as a function of magnetic field for Rb^{87} and Rb^{85}. Experimental data for Rb^{87} is marked with black circles, and Rb^{85} with inverted triangles. Linear fits are indicated by a red line for Rb^{87} and a blue line for Rb^{85}, fitting to equation 12 and resulting in Gyromagnetic ratios of $2.07 \times 10^{-5} \pm 0.03 \times 10^{-5}$ for Rb^{87} and $3.0 \times 10^{-5} \pm 0.2 \times 10^{-5}$ for Rb^{85}. Intercepts are 290.3 ± 0.1 for Rb^{87} and 445.8 ± 0.2 for Rb^{85}.

theoretical predictions, affirming the accuracy of our experimental techniques and findings.

References

[1] Optical pumping, 2023.

[2] Wikipedia contributors. Total angular momentum quantum number, 2023.

[3] MIT. Measuring optical pumping of rubidium vapor, 2023.

[4] MIT. Optical pumping of rubidium vapor, 2023.

[5] R. Paschotta. Optical pumping, 2023.

[6] Darren Puigh. Experiment s-10: Optical pumping. https://faculty.kfupm.edu.sa/phys/aanaqvi/OpticalPumping-cornell.pdf, 2006. Physics 510, Dated: February 27, 2006.

[7] TeachSpin. Optical pumping, 2023.

[8] Boston University. Optical pumping of rubidium, 2023.